Computer Modeling in
Engineering & Sciences

Tech Science Press

DOI: 10.32604/cmes.2023.027595

ARTICLE

Performance Analysis of Three Spectrum Sensing Detection Techniques with Ambient Backscatter Communication in Cognitive Radio Networks

Shayla Islam[1], Anil Kumar Budati[1,*], Mohammad Kamrul Hasan[2], Saoucene Mahfoudh[3] and Syed Bilal Hussian Shah[3]

[1]Institute of Computer Science & Digital Innovation, ICSDI, UCSI University, Kuala Lumpur, 56000, Malaysia

[2]Center for Cyber Security, Faculty of Information Science and Technology, Universiti Kebangsaan Malaysia (UKM), Selangor, 43600, Malaysia

[3]School of Engineering, Computing and Informatics, Dar Al-Hekma University, Jeddah, 22246, Saudi Arabia

*Corresponding Author: Anil Kumar Budati. Email: anilbudati@gmail.com

Received: 05 November 2022 Accepted: 29 December 2022

ABSTRACT

In wireless communications, the Ambient Backscatter Communication (AmBC) technique is a promising approach, detecting user presence accurately at low power levels. At low power or a low Signal-to-Noise Ratio (SNR), there is no dedicated power for the users. Instead, they can transmit information by reflecting the ambient Radio Frequency (RF) signals in the spectrum. Therefore, it is essential to detect user presence in the spectrum for the transmission of data without loss or without collision at a specific time. In this paper, the authors proposed a novel Spectrum Sensing (SS) detection technique in the Cognitive Radio (CR) spectrum, by developing the AmBC. Novel Matched Filter Detection with Inverse covariance (MFDI), Cyclostationary Feature Detection with Inverse covariance (CFDI) and Hybrid Filter Detection with Inverse covariance (HFDI) approaches are used with AmBC to detect the presence of users at low power levels. The performance of the three detection techniques is measured using the parameters of Probability of Detection (P_D), Probability of False Alarms (P_{fa}), Probability of Missed Detection (P_{md}), sensing time and throughput at low power or low SNR. The results show that there is a significant improvement via the HFDI technique for all the parameters.

KEYWORDS

Ambient backscatter communication; cognitive radio; MFDI; CFDI; HFDI

1 Introduction

In wireless CR networks, AmBC supports the detection of the Primary User (PU)/Primary Transmitter (PT) and Secondary User (SU)/Secondary Transmitter (ST) by estimating the spectrum availability for SU data transmission. The throughput performance of the SU is greatly improved compared to that of the PU [1–3]. The promising technology of AmBC can facilitate sustainable communication systems that do not depend on a dedicated carrier emitter. In the present paper, a novel framework is proposed for CR networks, with the support of AmBC. For Harvest-Then-Transmit (HTT) operations, an opportunistic SS framework is migrated with AmBC. The parameters of throughput, energy efficiency and energy consumption are measured to estimate framework performance [2–4]. A hybrid transmitter is developed by combining AmBC with the Internet of Things (IoT) [5–7]. A new spectrum sharing method is proposed by developing AmBC to enable it to estimate the entire RF spectrum. The Direct Link Interface (DLI) means that there are significant errors in the legacy spectrum. To minimize these errors, Conventional Energy Detection (CED) is proposed as a novel, statistical, clustering framework [8–11]. AmBC technology is used to estimate the spectrum slot by detecting signals across the CR spectrum. Two closed form detection thresholds are estimated using detection algorithms. The bit error rate is estimated using the probabilities of 0 or 1 at low and high SNR levels [12–15]. Integrating AmBC into RF-powered CR networks has been shown to be a promising method for achieving energy and spectrum efficient communications, which is very attractive for low-power or no-power communications. In such scenarios, a PU/SU can operate in either transmission mode or backscatter mode. Specifically, an SU can directly transmit data if sufficient energy has been harvested (i.e., transmission mode) or an SU can backscatter ambient signals to transmit data (i.e., backscatter mode). It has been demonstrated that integrating AmBC into RF-powered CRN is a promising strategy for achieving energy and spectrum efficiency in communications, which is very attractive for low-power or no-power communications. An SU can operate in either backscatter mode or transmission mode in these situations. Specifically, if sufficient energy has been harvested, an SU can transmit data directly (i.e., transmission mode) or an SU can backscatter ambient signals to transmit data (i.e., backscatter mode) [16–18] in order to provide security to quasi-passive CR communications in the electromagnetic spectrum and to activate incoming signals using real-time systems. This can be achieved by SS techniques with AmBC low power and efficient spectrum utilization, with the support of the semi-passive adaptive modulation technique. No additional spectral energy is added for quasi-passive opportunistic communication [19–21]. AmBC is a promising technology to support IoT by enabling low power operations like Wi-Fi and TV signals. However, it is more difficult to decode the backscatter signals with AmBC enabled networks and AmBC devices, rather than legacy receivers. Some Machine Learning (ML) based techniques are being developed to assist the AmBC signal detection [22–24].

The present paper focuses on how to estimate user presence more quickly and accurately with high throughput. To estimate channel availability in the CR spectrum, AmBC is used with MFDI, CFDI and HFDI computational modelling techniques. As the channel is not uniform, the radiated power is not uniform across the entire spectrum. We estimate a dynamic threshold for each channel, based on AmBC at a low power level. An analysis of three proposed SS detection techniques involves the Generalized Likelihood Ratio Test (GLRT). The key parameters for sensing the channel and measuring the accuracy of data received by end users are sensing time and throughput. Additive White Gaussian Noise (AWGN) is considered with non-uniform noise in the AmBC environment, to sense the channel and estimate the dynamic threshold. The performance of the three techniques is analysed for the parameters of P_D, P_{fa}, P_{md}, sensing time and throughput, and the best detection technique is identified. In wireless communication, environmental noise is not uniform and should vary depending on the parameters of temperature, humidity, pressure, etc. These variations are different at different frequency levels and the propagation loss/attenuation varies considerably in terms of different frequency levels. Therefore, in this paper, the authors considered a non-uniform AWGN to estimate the threshold for each channel. If the threshold value is not estimated properly, errors in relation to P_{fa} and P_{md} arise.

2 Proposed Methods

To estimate whether a channel in the spectrum is free or busy, two hypotheses can be written to assume that only noise is present (1) or that both user and noise are present (2) [7]. These hypotheses are represented as:

$$H_0 = y(n) = w(n) \tag{1}$$

$$H_1 = y(n) = s(n) + w(n) \tag{2}$$

where H_0 denotes the condition in which the spectrum slot is vacant and only AWGN (represented by w(n)) is exhibited. User presence in the spectrum slot is shown in the scenario, H_1, where the original signal is represented by s(n) and the noise signal by w(n).

In wireless communications, various noise levels are considered to exist in each channel. Therefore, the threshold for each power/SNR level must be estimated and the threshold changes dynamically, depending on the received SNR. To estimate the threshold for each channel, 'N', a jointly Gaussian random variable [7] is given as:

$$\mathrm{P}(\mathrm{y}; H_i) = \frac{1}{(2\pi\sigma^2)^{N/2}\det(C)^{1/2}}\exp\left[-\frac{1}{2}(y-H_i)^T C^{-1}(y-H_i)\right] \tag{3}$$

where C^{-1} is the inverse covariance, T is the transpose of the signal and H_i is H_0 or H_1. The 5G spectrum bands are the closest to the satellite frequency bands, i.e., they have frequency values in the tens of GHz. To estimate the threshold value in the 5G spectrum for user presence and absence, GLRT detection criteria are used. The GLRT threshold estimation condition [8] is:

$$L(y) = \frac{P(y; H_1)}{P(y; H_0)} = \gamma \tag{4}$$

2.1 MFDI

In the MFDI method, the threshold value in the decision-making device determines how the Matched Filter (MF) will be used to make decisions. The cellular radio ecosystem contains near-end and far-end consumers. High SNR signals are received by near-end users, whereas low SNR signals are received by far-end users. It is vital to estimate user presence below the cellular spectrum threshold. If the threshold value is static and high, at a low SNR, no user can be detected, i.e., P_{fa}. Alternatively, if the threshold value is low, then powerful noise signals cross the threshold and indicate a user's presence, i.e., P_{md}. Therefore, threshold estimate is the crucial factor in effectively identifying user presence. We developed a dynamic threshold estimation equation and the best threshold value is determined using the GLRT detection criteria. Different users have different fading conditions and propagation path losses. To estimate the dynamic threshold, a non-uniform AWGN is considered. The received signal is fed through an analogue-to-digital converter and the digital signal, x(n), is used as the input to the MF (Fig. 1). The MF maximizes the signal and suppresses the noise. The output of the MF, y(n), is analysed via GLRT, using the Least Square (LS) method to estimate the threshold. The threshold condition for MFDI with GLRT (MFDIG) is [9]:

$$L(Y) = (H_1 - H_0)^T C^{-1} y \gtrless \left[\ln(\gamma) + \frac{1}{2}\left((H_1 - H_0)^T C^{-1}(H_0 + H_1)\right)\right] * \left[hS^T + W\right] \tag{5}$$

where W is the M × N noise matrix, h is an LS estimator for the desired channel and S is the spectrum slots/channels $[s_1, s_2, \ldots, s_N]^T$.

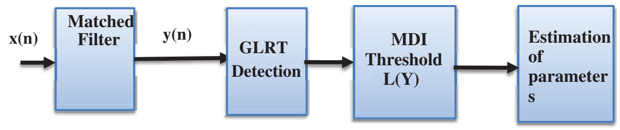

Figure 1: MFDI spectrum sensing technique

2.2 CFDI

In the CFDI method, the received signal, y(n), serves as the input to the N-point Fast Fourier Transform (FFT) (Fig. 2). The FFT is used for discrete spectral analysis to determine the frequency content of the signal. FFT has been used to achieve computational efficiency by adopting a 'divide-and-conquer' approach. A correlator is used to compare the threshold value of the current sample with that of the preceding sample, using the FFT signal output. If the values match, the current sample is used. If they do not match, the current sample is sent for further analysis. The threshold condition for CFDI with GLRT (CFDIG), using the LS method, is [10]:

$$R_{yy*}^{\propto} = \left[\ln(\gamma) + \frac{1}{2}\left((H_1 - H_0)^T C^{-1} (H_0 + H_1)\right) \exp(-j2\pi\alpha n f_s)\right]^{1/2} * \left[hS^T + W\right] \tag{6}$$

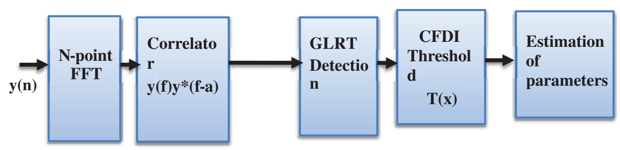

Figure 2: CFDI spectrum sensing technique

2.3 HFDI

In CFDI, the unfiltered input sample of the received signal is applied directly to the N-point FFT [11]. Due to the unfiltered input signal, P_D might be low at the detection level. The MF simultaneously increases the signal component and suppresses the noise amplitude. We attempted to combine the two detection algorithms of MFDI and CFDI into HFDI. The proposed HFDI block diagram is shown in Fig. 3.

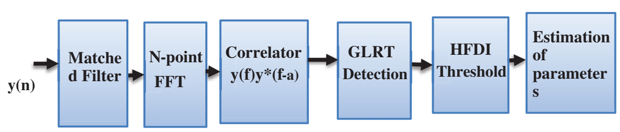

Figure 3: HFDI spectrum sensing technique

The samples received by the HFDI receiver are applied to MF, as y(n). At some point in time, the MF enhances the signal component and decreases the noise amplitude. The N-point FFT input is combined with the MF output. The frequency domain signal from the FFT is applied to a correlator, which compares previous samples to the results of the N-point FFT. If the values match, the current sample is used. If the new samples do not correlate with the previous samples, they are further analysed via a threshold detector. The dynamic threshold is computed for the proposed HFDI using GLRT detection criteria (HFDIG) with the LS method [12]:

$$L(Y) = \frac{(H_1 - H_0)}{\sigma^2} * \left[\ln(\gamma) + \frac{1}{2}\left((H_1 - H_0)^T C^{-1} (H_0 + H_1)\right) \exp(-j2\pi\alpha n f_s)\right] * \left[hS^T + W\right] \quad (7)$$

3 Performance Evaluation Metrics

To analyse the performance of the detection system, the following parameters are considered [11]: During SS, the channel/sample energy was detected and given to the comparator to check the threshold level. If the detected sample energy was above the threshold level, the user was presented in the spectrum slot. If the sample energy was less than the threshold level, the spectrum was identified as vacant. Threshold level played a vital role in identifying user presence in the spectrum. Accurate information was estimated for the spectrum by the parameter P_D. Hence, P_D was estimated using Eq. (8).

$$P_{fa} = Q\left(\frac{\gamma - (H_1 - H_0)^T C^{-1} H_0}{\sqrt{(H_1 - H_0)^T C^{-1} (H_1 - H_0)}}\right) \quad (8)$$

If the user was located far away from the cell tower or in the overlay region, a weak signal was received and the SNR value recorded almost negative decibels. At a low SNR, noise domination was increased, or the noise signal energy was higher than the original signal power. In this case, the threshold value was low, the strongly noise dominated signal crossed the threshold and the decision was made that the user was present, however, there was no user. This type of wrong detection is referred to as P_{fa}. These false alarms are estimated using Eq. (9):

$$P_D = Q[Q^{-1}\left(P_{fa}\right) - \sqrt{(H_1 - H_0)^T C^{-1} (H_1 - H_0)} \quad (9)$$

If the user was located far away from the cell tower or in the overlay region, a weak signal was received, and the SNR value recorded almost negative decibels. At a low SNR, the noise domination was increased, or the noise signal energy was higher than the original signal power. In this case, the threshold value was high, the signal did not cross the threshold and the decision was made that the user was absent, however, there was no user. These inaccurate detections are known as P_{md} and are estimated using Eq. (10):

$$P_{md} = Q\left(\frac{\gamma - (H_1 - H_0)^T C^{-1} H_1}{\sqrt{(H_1 - H_0)^T C^{-1} (H_1 - H_0)}}\right) \quad (10)$$

Throughput is an important parameter, the improvement of which entirely depends on quicker sensing of the spectrum to allow more time for data transmission. In this paper, we considered both the PU and the SU. In Fig. 4, T_F is the frame duration, T_S is the time to sense the channel, T_c is the time taken for the sensed information to be given to the fusion centre and T is the total sensing and decision time of the spectrum. The data transmission duration is, therefore, $T_F - (T_s + T_c)$. The throughput estimation with respect to a false alarm is:

$$T_{hf} = \frac{T_F - T}{T}\left(1 - P_{fa}\right) \quad (11)$$

$$T_{hd} = \frac{T_F - T}{T}(1 - P_D) \quad (12)$$

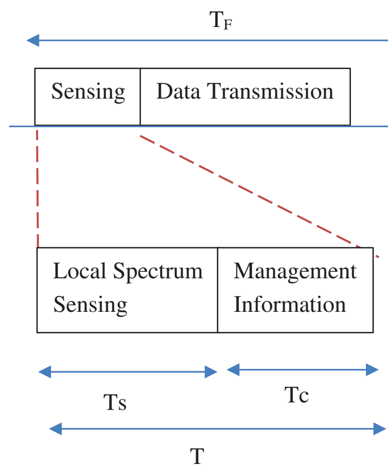

Figure 4: Spectrum sensing time representation

The data are not continuously transmitted in the spectrum; when the spectrum is scanning, data transmission should be in the ideal mode. Therefore, the time interval in data transmission is represented as β. The length of the frame transmitted in the spectrum is represented as T_{RF}:

$$T_{hf1} = \frac{T_F - T}{T} \left(1 - P_{fa}\right) e^{\left(-\frac{T_{RF}}{\beta}\right)} \tag{13}$$

$$T_{hd1} = \frac{T_F - T}{T} \left(1 - P_D\right) e^{\left(-\frac{T_{RF}}{\beta}\right)} \tag{14}$$

Sensing time is measured for the CR spectrum is:

$$T_s = tN \tag{15}$$

where T_s is the sensing time and N is the number of samples required for the CR system to achieve the target P_D of 100%.

4 Results

To test and validate the results, the authors have considered the assumptions with respect to the MATLab Simulator, which is shown in Table 1.

Table 1: Assumptions for simulation environment

Parameter	Assumption
Samples	1000
Noise environment	Non-uniform gaussian
Threshold	Dynamic
SNR range	0 to −10 dB
Modulation technique	BPSK

4.1 P_D

A comparison of the three proposed methods for parameter P_D is shown in Fig. 5. When the power level increases from −10 to 0 dB, the detection probability also increases. The best method shows a high P_D at low SNR values. At −10 dB, the detection probabilities are 0.45, 0.66 and 0.69 for CFDIG, MDIG and HFDIG, respectively, showing that the proposed HFDIG is superior. HFDIG and MDIG provide a high detection probability of 1 from −4 dB onwards, but the CFDIG only shows this performance at −1 dB.

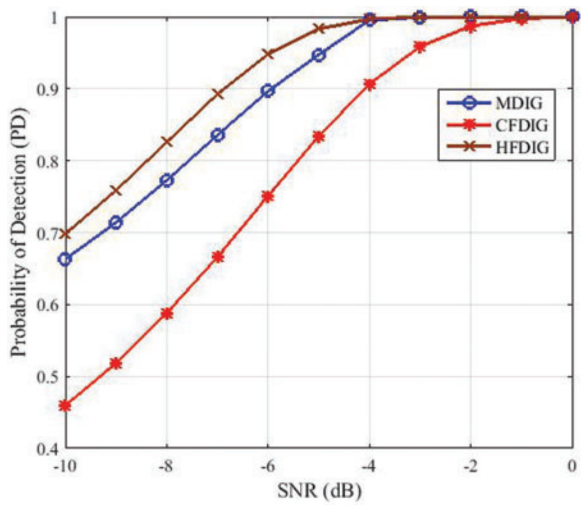

Figure 5: Comparison of P_D *vs.* input SNR

HFDIG and MDIG perform better than CFDIG at low SNR values. From −10 to −4 dB, HFDIG provides a higher detection probability than MDIG at all SNR values. The proposed HFDIG is, therefore, superior. The rate of increase of detection probability between the proposed three methods is shown in Fig. 6.

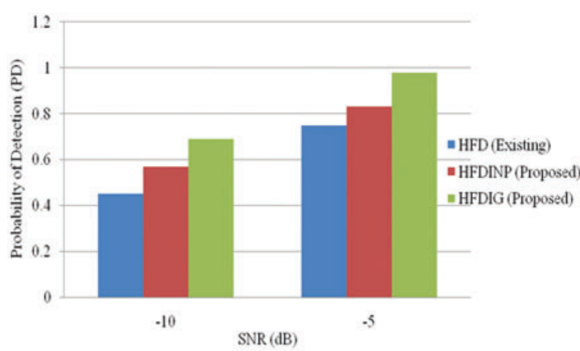

Figure 6: Comparison of performance on P_D using dynamic thresholds

If the threshold value is identified accurately, then there is a low detection probability. If the threshold level is changed according to the input SNR, there is a better chance of improving the detection probability than using the fixed threshold approach. The dynamic threshold approach provides more accurate detection than the fixed threshold approach for the parameter P_D. MDIG, CFDIG and HFDIG perform better than the existing methods. Fig. 6 shows the rate of increase of detection probability from −10 to −5 dB. At −10 dB, the detection probabilities of HFDIG, MDIG and CFDIG are 0.69, 0.66 and 0.45, respectively. At −5 dB, the detection probabilities of HFDIG, MDIG and CFDIG are 0.98, 0.94 and 0.83, respectively. Therefore, when the power level increases from −10 to −5 dB, the rate of increase of the detection probabilities for HFDIG, MDIG and CFDIG are 0.29, 0.28 and 0.38, respectively. CFDIG has the highest rate of increase in detection probability but performs less well at low SNR levels. HFDIG has higher detection probabilities overall, therefore, at a low SNR level, this is the best method when evaluated against the parameter P_D.

4.2 P_{fa}

A comparison of the three proposed methods for the parameter P_{fa} is shown in Fig. 7. When the power level increases from −10 to 0 dB, P_{fa} decreases. The best method gives a low P_{fa} at low SNR values. At −10 dB, the P_{fa} is 0.48, 0.33 and 0.30 for CFDIG, MDIG and HFDIG, respectively, meaning that HFDIG offers the lowest probability of showing a false alarm. HFDIG and MDIG show almost zero false alarms from −4 dB onwards, but CFDIG only reaches its lowest probability (of 0.02) at 0 dB. HFDIG and MDIG show fewer false alarms than CFDIG at low SNR values and HFDIG indicates fewer false alarms than MDIG at all SNR values.

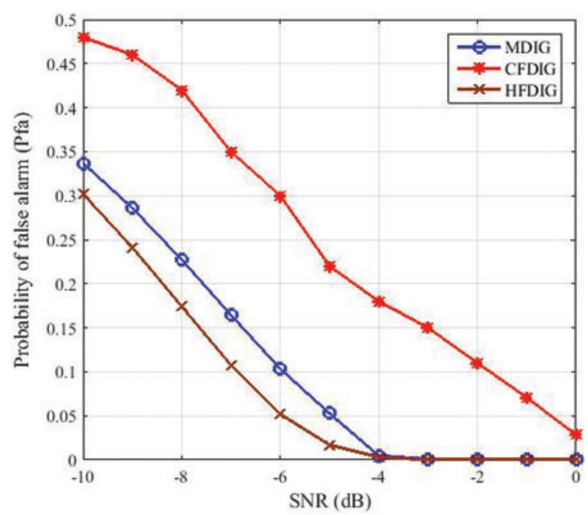

Figure 7: Comparison of P_{fa} *vs.* input SNR

The rate of decrease in false alarm probability for the three methods is shown in Fig. 8. If the fixed threshold value is low, then there is a high probability of generating false alarms. If the threshold level is changed according to the input SNR, then the false alarm performance will also change. In terms of the dynamic threshold, MDIG, CFDIG and HFDIG provide better detection than existing methods. The performance analysis for P_{fa} is shown in Fig. 8. At −10 dB, the false alarm probabilities of HFDIG, MDIG and CFDIG are 0.30, 0.33 and 0.48, respectively; at −5 dB, the probabilities are 0.01, 0.05 and 0.22, respectively. Therefore, when the power level is increased from −10 to −5 dB, the decreases in false alarm probability for HFDIG, MDIG and CFDIG are 0.29, 0.28 and 0.26, respectively. HFDIG has the highest rate of decrease of P_{fa} and shows fewer false alarm probabilities at low SNR levels. It is, therefore, the superior detection method at lower SNR values, when evaluated against the P_{fa} parameter.

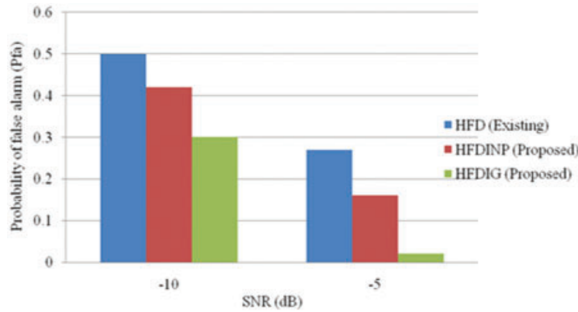

Figure 8: Comparison of performance on P_{fa} using dynamic thresholds

4.3 P_{md}

A comparison of the three proposed methods for the parameter, P_{md}, is shown in Fig. 9. As the power level increases from −10 to 0 dB, the P_{md} decreases. The best detection method is the one that offers the lowest P_{md} at low SNR values. At −10 dB, the P_{md} is 0.54, 0.40 and 0.37 for CFDIG, MDIG and HFDIG, respectively. The proposed HFDIG shows superior performance. HFDIG and MDIG show almost zero missed detections from −4 dB onwards, but CFDIG only shows zero from −1 dB onwards. HFDIG and MDIG, therefore, they provide superior missed detection over CFDIG at low SNR values. Between −10 and −4 dB, HFDIG performs better than MDIG across all SNR values.

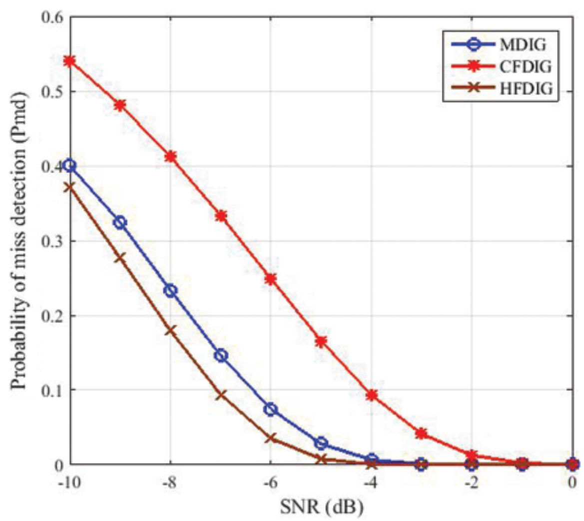

Figure 9: Comparison of P_{md} *vs.* input SNR

The rate of decrease of P_{md} in all three methods is shown in Fig. 10. If the fixed threshold value is high, then there is a high P_{md}. If the threshold level changes according to the input SNR, missed detection performance will also change. The dynamic threshold leads to more accurate detection, as MDIG, CFDIG and HFDIG offer less missed detection than the existing method (Fig. 11).

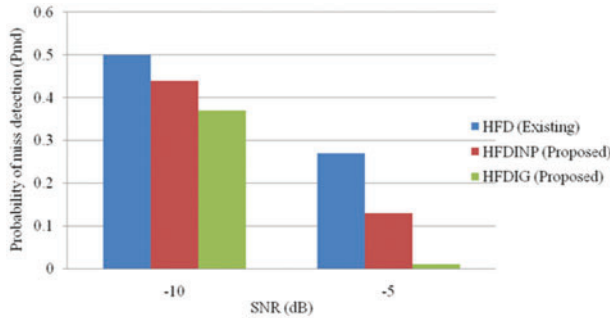

Figure 10: Comparison of performance on P_{md} using dynamic thresholds

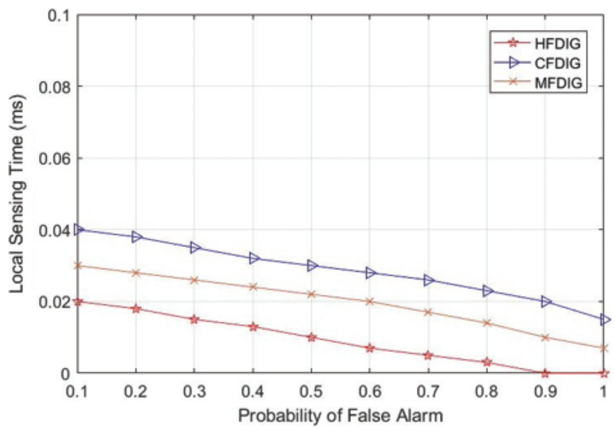

Figure 11: Local sensing time *vs.* probability of false alarm at SNR $= -10$ dB

At -10 dB, the P_{md} of HFDIG, MDIG and CFDIG is 0.37, 0.40 and 0.54, respectively; at -5 dB, the probabilities are 0.01, 0.02 and 0.16, respectively. Therefore, when the power level increases from -10 to -5 dB, the rates of decrease of P_{md} for HFDIG, MDIG and CFDIG are 0.36, 0.38 and 0.38, respectively. MDIG and CFDIG show equal rates of decrease in missed detection in relation to HFDIG. At a low SNR level, HFDIG has fewer missed detection probability levels and shows greater improvement. Hence, HFDIG is the superior method when evaluated against the missed detection parameter.

Fig. 11 represents the sensing time in milliseconds (ms) *vs.* the probability of a false alarm at an SNR of -10 dB. HFDIG is quicker than the other two techniques, saving 0.01 and 0.02 ms by comparison with MFDIG and CFDIG, respectively, when $P_{fa} = 0.1$.

Fig. 12 represents the sensing time (ms) *vs.* the P_D at an SNR of -10 dB. HFDIG is quicker than the other two techniques, saving 0.1 and 0.14 ms in relation to MFDIG and CFDIG, respectively, when $P_D = 1$.

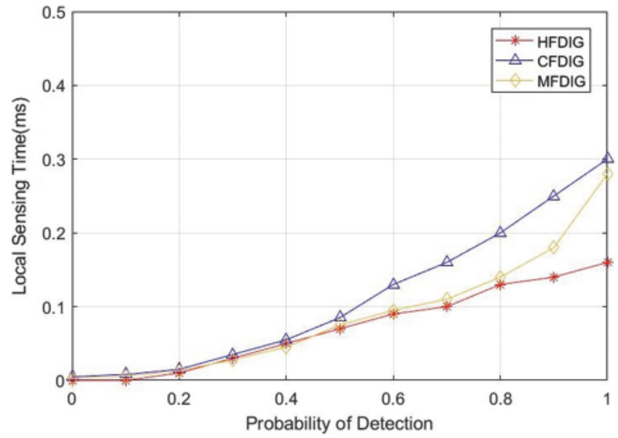

Figure 12: Local sensing time *vs.* probability of detection at SNR $= -10$ dB

HFDIG shows superior performance according to P_D, P_{fa}, P_{md} and sensing time. Therefore, throughput is estimated for HFDIG at various lambda values.

Fig. 13 shows the normalized throughput *vs.* the P_{fa} at various data transmission times, shown as beta (β) values. The P_{fa} increases the β value exponentially, as per Eq. (13). Fig. 13 shows that $\beta = 500$ ms gives better throughput than $\beta = 400$ ms and $\beta = 450$ ms. Therefore, when β is increased, throughput also increases.

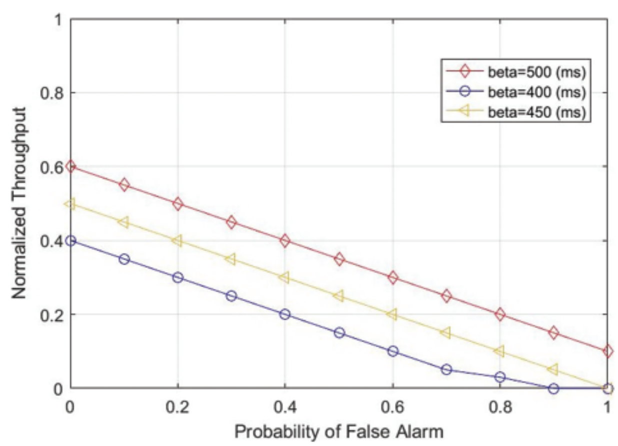

Figure 13: Normalized throughput *vs.* probability of false alarm

5 Conclusion

The present research has compared the performance of AmBC technology with HFDIG, MFDIG and CFDIG computing modelling techniques by setting against the parameters of P_D, P_{fa}, P_{md}, local sensing time and throughput. HFDIG exhibits superior performance across all parameters and there is an improvement in detection, false alarms and missed detection of 3%, 3% and 4%, respectively. Compared with HFDIG, the local sensing time of CFDIG and MFDIG is improved by 3% and 2% at Pfa = 0.5, and the local sensing time of CFDIG and MFDIG is improved by 2% and 4 % at PD

= 0.5. Hence, empty slots in the RF spectrum are sensed and identified more quickly and accurately with the proposed HFDIG.

Funding Statement: The authors would like to express their gratitude to the Ministry of Higher Education Malaysia for funding this research project through Fundamental Research Grant Scheme (FRGS) with Project Code: FRGS/1/2022/TK02/UCSI/02/1 and also to UCSI University, Malaysia and to the Vice Presidency for Graduate Studies, Business and Scientific Research (GBR) at Dar AI Hekma University, Jeddah, Saudi Arabia.

Conflicts of Interest: The authors declare that they have no conflicts of interest to report regarding the present study.

References

1. Munir, D., Shah, S. T., Choi, K. W., Lee, T. J., Chung, M. Y. (2019). Performance analysis of wireless-powered cognitive radio networks with ambient backscatter. *EURASIP Journal on Wireless Communications and Networking, 2019(1),* 1–13. https://doi.org/10.1186/s13638-019-1367-7
2. Kishore, R., Gurugopinath, S., Sofotasios, P. C., Muhaidat, S., Al-Dhahir, N. (2019). Opportunistic ambient backscatter communication in RF-powered cognitive radio networks. *IEEE Transactions on Cognitive Communications and Networking, 5(2),* 413–426. https://doi.org/10.1109/TCCN.6687307
3. Zhuang, Y., Li, X., Ji, H., Zhang, H., Leung, V. C. (2020). Optimal resource allocation for RF-powered underlay cognitive radio networks with ambient backscatter communication. *IEEE Transactions on Vehicular Technology, 69(12),* 15216–15228. https://doi.org/10.1109/TVT.25
4. Lu, X., Niyato, D., Jiang, H., Kim, D. I., Xiao, Y. et al. (2018). Ambient backscatter assisted wireless powered communications. *IEEE Wireless Communications, 25(2),* 170–177. https://doi.org/10.1109/MWC.2017.1600398
5. Guo, H., Zhang, Q., Xiao, S., Liang, Y. C. (2018). Exploiting multiple antennas for cognitive ambient backscatter communication. *IEEE Internet of Things Journal, 6(1),* 765–775. https://doi.org/10.1109/JIOT.2018.2856633
6. Wang, G., Gao, F., Fan, R., Tellambura, C. (2016). Ambient backscatter communication systems: Detection and performance analysis. *IEEE Transactions on Communications, 64(11),* 4836–4846. https://doi.org/10.1109/TCOMM.2016.2602341
7. Tertinek, S. (2004). Optimum detection of deterministic and random signals. *Advanced Signal Processing 1 SE,* 1–6.
8. Gong, S., Wang, P., Liu, W. (2012). Spectrum sensing under distribution uncertainty in cognitive radio networks. *2012 IEEE International Conference on Communications (ICC)*, pp. 1512–1516. Cultural Center of Ottawa, Canada, IEEE.
9. Budati, A. K., Valiveti, H. (2022). Identify the user presence by GLRT and NP detection criteria in cognitive radio spectrum sensing. *International Journal of Communication Systems, 35(2),* e4142. https://doi.org/10.1002/dac.4142
10. Kumar, B. A., Hima Bindu, V., Swetha, N. (2021). User detection using cyclostationary feature detection in cognitive radio networks with various detection criteria. *International Conference on Innovative Computing and Communications*, pp. 1013–1029. Singapore, Springer.
11. Maeda, K., Benjebbour, A., Asai, T., Furuno, T., Ohya, T. (2007). Recognition among OFDM-based systems utilizing cyclostationarity-inducing transmission. *2nd IEEE International Symposium on New Frontiers in Dynamic Spectrum Access Networks*, pp. 516–523. Dublin, Ireland, IEEE.

12. Budati, A. K., Ghinea, G., Ganesh, S. N. V. (2022). Novel aninath computation detection algorithm to identify the UAV users in 5G networks. *Wireless Personal Communications, 127,* 963–978. https://doi.org/10.1007/s11277-021-08459-3
13. Siddiqui, S. Y., Haider, A., Ghazal, T. M., Khan, M. A., Naseer, I. et al. (2021). IoMT cloud-based intelligent prediction of breast cancer stages empowered with deep learning. *IEEE Access, 9,* 146478–146491. https://doi.org/10.1109/ACCESS.2021.3123472
14. Ahmed, Z. E., Hasan, M. K., Saeed, R. A., Hassan, R., Islam, S. et al. (2020). Optimizing energy consumption for cloud Internet of Things. *Frontiers in Physics, 8,* 358.
15. Hasan, M. K., Islam, S., Memon, I., Ismail, A. F., Abdullah, S. et al. (2022). A novel resource oriented DMA framework for internet of medical things devices in 5G network. *IEEE Transactions on Industrial Informatics*. https://doi.org/10.1109/TII.2022.3148250
16. Liu, H., Li, G., Li, X., Huang, G., Liu, Y. et al. (2022). Effective capacity analysis of STAR-RIS assisted NOMA networks. *IEEE Wireless Communications Letters, 11(9),* 1930–1934. https://doi.org/10.1109/LWC.2022.3188443
17. Zhang, Y., He, W., Li, X., Peng, H., Rabie, K. M. et al. (2022). Covert communication in downlink NOMA systems with channel uncertainty. *IEEE Sensors Journal, 22(19),* 19101–19112. https://doi.org/10.1109/JSEN.2022.3201319
18. Li, X., Zheng, Y., Zeng, M., Liu, Y., Dobre, O. A. (2022). Enhancing secrecy performance for STAR-RIS NOMA networks. *IEEE Transactions on Vehicular Technology*. https://doi.org/10.1109/TVT.2022.3213334
19. Hasan, M. K., Akhtaruzzaman, M., Kabir, S. R., Gadekallu, T. R., Islam, S. et al. (2022). Evolution of industry and blockchain era: Monitoring price hike and corruption using BIoT for smart government and Industry 4.0. *IEEE Transactions on Industrial Informatics*. https://doi.org/10.1109/TII.2022.3164066
20. Hasan, M. K., Alkhalifah, A., Islam, S., Babiker, N., Habib, A. K. M. et al. (2022). Blockchain technology on smart grid, energy trading, and big data: Security issues, challenges, and recommendations. *Wireless Communications and Mobile Computing, 2022*. https://doi.org/10.1155/2022/9065768
21. Hasan, M. K., Chuah, T. C., El-Saleh, A. A., Shafiq, M., Shaikh, S. A. et al. (2021). Constriction factor particle swarm optimization based load balancing and cell association for 5G heterogeneous networks. *Computer Communications, 180,* 328–337. https://doi.org/10.1016/j.comcom.2021.10.021
22. Xu, L., Zhu, K., Wang, R., Gong, S. (2018). Performance analysis of RF-powered cognitive radio networks with integrated ambient backscatter communications. *Wireless Communications and Mobile Computing, 2018*. https://doi.org/10.1155/2018/8509693
23. Purushothama, J. M., Ding, Y., Goussetis, G., Brookes, J. (2022). Low power secure backscatter communication techniques exploring ambient signals. *2022 Microwave Mediterranean Symposium (MMS)*, pp. 1–4. Pizzo Calabro, IEEE.
24. Toro, U. S., ElHalawany, B. M., Wong, A. B., Wang, L., Wu, K. (2021). Machine-learning-assisted signal detection in ambient backscatter communication networks. *IEEE Network, 35(6),* 120–125. https://doi.org/10.1109/MNET.001.2100247